Determination of Mass Transfer and Thermodynamic Properties of Branched Paraffins in Silicalite by Inverse Chromatography Technique

ARTICLE *in* INDUSTRIAL & ENGINEERING CHEMISTRY RESEARCH · JANUARY 2001

Impact Factor: 2.59 · DOI: 10.1021/ie0004693

4 AUTHORS, INCLUDING:

Elsa Jolimaître
IFP Energies nouvelles
22 PUBLICATIONS **461** CITATIONS
SEE PROFILE

Melaz Tayakout-fayolle
Claude Bernard University Lyon 1
73 PUBLICATIONS **439** CITATIONS
SEE PROFILE

K. Ragil
IFP Energies nouvelles
15 PUBLICATIONS **418** CITATIONS
SEE PROFILE

Determination of Mass Transfer and Thermodynamic Properties of Branched Paraffins in Silicalite by Inverse Chromatography Technique

E. Jolimaitre,*,† M. Tayakout-Fayolle,† C. Jallut,† and K. Ragil‡

Laboratoire d'Automatique et de Génie des Procédés, Université Claude Bernard et ESCPE Lyon, UPRES A Q 5007 CNRS, 43, boulevard du 11 novembre 1918, 69622 Villeurbanne Cedex, France, and Institut Français du Pétrole, 1 & 4 avenue de Bois-Préau, 92852 Rueil-Malmaison Cedex, France

Equilibrium isotherms and effective diffusivities of 3-methylpentane, isopentane, and 2,2-dimethylbutane were measured between 150 and 300 °C by a linear inverse chromatography technique. The validity of the equilibrium data was checked with gravimetric experiments, and both sets of data are in good agreement. The activation energies determined from the variation of the self-diffusivities with temperature lie in the range of literature results. The following trend was observed for the self-diffusivities: isopentane > 3-methylpentane > 2,2-dimethylbutane. The effective diffusivities of these compounds were found to increase with the adsorbed-phase loadings according to Darken's law for a loading ratio less than 0.7. Above this value, the diffusivities are higher than those given by Darken's law.

Introduction

Separation of double-branched paraffins from single-branched and normal paraffins is of great industrial interest, because of its potential applications in the octane number enhancement of fuel products. This separation is, however, particularly difficult because of the close thermodynamic properties of the compounds involved. Indeed, the boiling points of these compounds are very close, as are their adsorption capacities on most of the industrial adsorbents. Therefore, separation by distillation or by equilibrium-induced adsorption processes is not economically interesting. Separation induced by kinetic effects has been investigated[1,2] using zeolite ZSM-5 as a shape-selective adsorbent.

To evaluate the industrial feasibility of this separation, which seems to be promising, a very good knowledge of the physical properties of the system is needed, including the adsorption equilibria and the diffusivities of the paraffins in ZSM-5. In this paper are reported the measurement of these parameters in silicalite, the dealuminated form of ZSM-5, for three branched paraffins: isopentane, 3-methylpentane, and 2,2-dimethylbutane.

The measurements were made by the perturbation chromatography technique, or concentration pulse chromatography (CPC).[3−6] CPC has been widely used for parameter estimation purposes.[4,7−9] The basic principle of this method consists of injecting, at time zero and at the inlet of a fixed bed of the adsorbent, a pulse of one component diluted in the flow of an inert carrier (the input) and measuring the experimental response of the concentration at the outlet (the output). Initially, the bed can be fed either with pure inert carrier or with a mixture of inert carrier and adsorbate at constant inlet concentration, which will be called background composition. In both cases, the initial thermodynamic and thermal equilibrium is perturbed by the adsorbate concentration pulse.

If the adsorbate concentration variation at the column's inlet is low enough, one can consider that (1) the variation of temperature and velocity in the bed is negligible, (2) the adsorption equilibrium can be considered as linear, and (3) all of the transport parameters are constant.

Under these conditions, the system is linear with respect to the input, and the technique is called linear inverse chromatography. To estimate the parameters from experimental results, a linear model, valid only in the neighborhood of the initial equilibrium state, is used.

Once the model has been derived, a parameter estimation strategy must be selected. Two methods are commonly used in the literature to evaluate parameters from CPC curves: the method of moments[8,9] and time domain analysis.[5−7] The moments method consists of measuring the mean retention time (first moment) and the standard deviation (second moment) and comparing the experimental values with those derived from the model. This method is easy to use but has two major drawbacks: it is not always very accurate when the experimental responses are highly skewed, and it is inefficient at separating the effects of the different resistances to mass transfer.

Time domain analysis, which consists of finding the parameters by using an optimization technique, takes into account all of the information included in the response. It is therefore more precise than the method of moments and makes it possible, under strict conditions,[10] to separate the contributions of the different resistances. The main problem of time domain analysis is that it is an iterative method based on model numerical resolution and thus is quite time-consuming. Fahim and Wakao[11] found that a combination between the moment method and time domain fitting was the best: the moment method can be used to obtain the

* Corresponding author. Telephone: 33 1 47 52 56 15. Fax: 33 1 47 52 70 25. E-mail: elsa.jolimaitre@ifp.fr.
† Université Claude Bernard et ESCPE Lyon.
‡ Institut Français du Pétrole.

10.1021/ie0004693 CCC: $20.00
Published on Web 01/06/2001

initial values of the parameters for the global and final time domain optimization.

In this paper, both methods will also be used, but in quite a different way. The method of moments will be used to extract equilibrium and mass transfer parameters from response curves. Time domain fitting will be used to verify that the micropore diffusion is the limiting step (by performing a sensitivity study) and to estimate the parameters related to the macropore mass transfer step.

Model

Model Assumptions. The linear model developed here for parameter estimation is based on the following assumptions: (1) Adsorption equilibrium is linear. (2) The system is isothermal. (3) The velocity of the fluid in the column does not vary. (4) Diffusion in the micropore is represented by the Fick equation with constant micropore diffusivity. (As mentioned before, these four first assumptions are reasonable only if the variation in concentration in the column is small.) (5) Adsorbent has a bidisperse pore structure. The crystals of silicalite used in this study have a mean radius of 2 μm. To minimize the pressure drop, these crystals were agglomerated to form particles. The macropore diffusional resistance was taken into account in the model. However, because the micropore resistance is supposed to be the limiting step in a kinetic separation, a complete description of macropore diffusion did not seem to be necessary. The macropore resistance is therefore lumped: concentration in the macropore is assumed to be uniform, and an additional mass transfer coefficient k_t is introduced at the surface of the crystals. (6) The flow pattern is described by the axial dispersed plug flow model. Axial dispersion, which is usually negligible in industrial units, is taken into account in our model, because of the small size of the column and the small interstitial velocity. (7) For the same reasons, the frictional pressure drop is negligible. (8) An external film resistance between the fluid phase and the surface of the particles is taken into account. (9) Only one component is adsorbed.

Equations. The model equations are derived from mass balances for the three porosity levels of the bed, subject to the above-discussed assumptions. The concentrations appearing in this model are defined as the difference between their current values and their values at the initial thermodynamic equilibrium state: $\hat{C} = C - \bar{C}$, $\hat{q} = q - \bar{q}$.

Fluid Phase

$$\frac{\partial \hat{C}}{\partial t} = D_L \frac{\partial^2 \hat{C}}{\partial z^2} - v \frac{\partial \hat{C}}{\partial z} - \left(\frac{1-\epsilon_i}{\epsilon_i}\right)\frac{3k_p}{R_p}(\hat{C} - \hat{C}_p) \quad (1)$$

Boundary Conditions

$$\left.\frac{\partial \hat{C}}{\partial z}\right|_{z=L} = 0 \quad (2)$$

$$D_L \left.\frac{\partial \hat{C}}{\partial z}\right|_{z=0} = -v(\hat{C}|_{z=0} - \hat{C}|_{z=0+}) \quad (3)$$

Macropore Mass Balance

$$\frac{\partial \hat{C}_p}{\partial t} = \frac{3k_p}{R_p \epsilon_p}(\hat{C} - \hat{C}_p) - \left(\frac{1-\epsilon_p}{\epsilon_p}\right)\frac{3k_t}{R_c}(\hat{C}_p - \hat{C}_p|_{r_c=R_c}) \quad (4)$$

Crystal Mass Balance

$$\frac{\partial \hat{q}}{\partial t} = \frac{1}{r_c^2} D_c \frac{\partial \hat{q}}{\partial r_c}\left(r_c^2 \frac{\partial \hat{q}}{\partial r_c}\right) \quad (5)$$

Boundary Conditions

$$\left.\frac{\partial \hat{q}}{\partial r_c}\right|_{r_c=0} = 0 \quad (6)$$

$$D_c \left.\frac{\partial \hat{q}}{\partial r_c}\right|_{r_c=R_c} = k_t(\hat{C}_p - \hat{C}_p|_{r_c=R_c}) \quad (7)$$

Thermodynamic Equilibrium Conditions

$$q|_{r_c=R_c} = q^* = K_a C_p|_{r_c=R_c} \quad (8)$$

K_a being the slope of the equilibrium curve at the initial equilibrium state.

The first and second moment corresponding to this model are[12]

$$\mu_1 = \frac{L}{v}\left[1 + \left(\frac{1-\epsilon_i}{\epsilon_i}\right)K\right] \quad (9)$$

$$\mu_2^c = 2\mu_1^2\left[\frac{D_L}{vL} + \left(\frac{v}{L}\right)\left(\frac{\epsilon_i}{1-\epsilon_i}\right)\left(\frac{R_p}{3k_p} + \frac{R_c}{3k_t} + \frac{R_c^2}{15KD_c}\right) \times \left(1 + \frac{\epsilon_i}{(1-\epsilon_i)K}\right)^{-2}\right] \quad (10)$$

$$K = \epsilon_p + (1-\epsilon_p)K_a \quad (11)$$

Equation 10 is valid only if $K \gg \epsilon_p$, which is usually true. Equations 9−11 are used within the framework of the moments method.

Identifiability Considerations for Time Domain Analysis. Equations 1−8 constitute the linear chromatographic column model. They contain 11 parameters: L, v, ϵ_i, ϵ_p, k_p, k_t, D_c, D_L, R_p, R_c, and K_a. It is well-known that, given only the structure of the model and independently of the experimental results, all of those parameters cannot be estimated from a chromatographic experiment; they are not all structurally identifiable.[13]

The structural identifiability of the parameters of linear inverse chromatography models was studied by Tayakout-Fayolle et al.,[10] and it was shown that only the groups of parameters contained in the transfer function (or any other set of parameters resulting of their combination) are structurally identifiable. In our case, for a bidisperse model, only seven groups of parameters, named C_1−C_7 and listed in Table 1, are structurally identifiable. This means that only C_1−C_7 would appear in the analytical solution for the column response. Hence, these and only these groups (or a combination of these groups) can be estimated. Consequently, the time domain linear model must be formulated in such a way that only these seven groups are present in the equations. Tayakout-Fayolle et al.[10] showed that this can be achieved only if: (1) equations are written in dimensionless form by introducing new dimensionless space variables $\zeta = x/L$ and $\rho = r_c/R_c$, and (2) the state variable describing the adsorbent composition is changed according to $C_p^*(r_c,t) = [q(r_c,t)/K_a]$.

Table 1. Structurally Identifiable Parameter Groups of the Linear Chromatography Model

	time constants	volume ratios
fluid phase	$C_1 = \frac{L^2}{D_L}$	
	$C_2 = \frac{L}{v}$	
particle	$C_3 = \frac{R_p \epsilon_p}{k_p}$	$C_4 = \left(\frac{1-\epsilon_i}{\epsilon_i}\right)\epsilon_p$
crystals	$C_5 = \frac{R_c^2}{D_c}$	$C_6 = \left(\frac{1-\epsilon_p}{\epsilon_p}\right)K_a$
	$C_7 = \frac{R_c K_a}{k_t}$	

Equations 1−8 then become

Fluid Phase

$$\frac{\partial \hat{C}}{\partial t} = \frac{1}{C_1}\frac{\partial^2 \hat{C}}{\partial \xi^2} - \frac{1}{C_2}\frac{\partial \hat{C}}{\partial \xi} - 3\frac{C_4}{C_3}(\hat{C} - \hat{C}_p) \qquad (12)$$

Boundary Conditions

$$\left.\frac{\partial \hat{C}}{\partial \xi}\right|_{\xi=1} = 0 \qquad (13)$$

$$\left.\frac{\partial \hat{C}}{\partial \xi}\right|_{\xi=0} = -\frac{C_1}{C_2}(\hat{C}|_{\xi=0-} - \hat{C}|_{\xi=0+}) \qquad (14)$$

Particle Mass Balance

$$\frac{\partial \hat{C}_p}{\partial t} = \frac{3}{C_3}(\hat{C} - \hat{C}_p) - 3\frac{C_6}{C_7}(\hat{C}_p - \hat{C}_p^*|_{\rho=1}) \qquad (15)$$

Crystal Mass Balance

$$\frac{\partial \hat{C}_p^*}{\partial \rho} = \frac{1}{C_5 \rho^2}\frac{\partial}{\partial \rho}\left(\rho^2 \frac{\partial \hat{C}_p^*}{\partial \rho}\right) \qquad (16)$$

Boundary Conditions

$$\left.\frac{\partial \hat{C}_p^*}{\partial \rho}\right|_{\rho=0} = 0 \qquad (17)$$

$$\left.\frac{\partial \hat{C}_p^*}{\partial \rho}\right|_{\rho=1} = \frac{C_5}{C_7}(C_p - C_p^*|_{\rho=1}) \qquad (18)$$

Equations 12−18 are the final form of the model used for parameter estimation using the time domain analysis. Once the parameter groups C_1−C_7 have been estimated by means of an optimization technique, the physical parameters are calculated from the expressions of the groups written in Table 1. Because there are 7 groups and 11 parameters, 4 parameters have to be known so that the others can be calculated. Those parameters are the length of the bed L, the mean radius of the crystal R_c, the mean radius of the particles R_p, and the fluid superficial velocity $u = v\epsilon_i$.

Method of Solution for the Time Domain Analysis. The dimensionless eqs 12−18 were written in the collocation form, thus reducing the set of partial differential equations to a set of algebraic and ordinary differential equations.

These equations were then numerically integrated using the IMSL DASPG routine, based on Petzold-Gear's integration method. Between 10 and 25 interval points were needed along the length of the bed, depending on the stiffness of the solution, and 5 points were needed along the crystal radius (see Jolimaitre[14]). Parameter estimation was performed using the IMSL BCLSF routine and minimizing a least-squares criteria between calculated and measured outlet concentrations.

Experimental Section

Adsorbent Characterization. The silicalite crystals used in this study are taken from a single sample, which was supplied by Zeolist International. Its Si/Al ratio, measured by X-ray fluorescence, is 500 ± 50%. The mean crystal diameter is $R_c = 2 \times 10^{-6}$ m.

Particles were made by extrusion with a binder (silica) in the Institut Français du Pétrole. Extrudates are small cylinders with a diameter of 1 mm and a mean length of 4 mm. For model simplification, particles were supposed to be spherical with a mean radius of 1 mm, the radius of a sphere having the same surface area as the particle.

The ratio of binder in the particles

$$t = \frac{\text{mass of binder}}{\text{mass of particle}} = 0.44 \qquad (19)$$

was determined by gravimetric uptake measurements (made in the Institut Français du Pétrole), by comparing the quantity of 3-methylpentane adsorbed in crystals and in particles, for three different temperatures. Activation of the adsorbent was performed by raising the temperature to 450 °C for 4 h.

Experimental Setup. A schematic of the gas chromatography apparatus used in this study is presented in Figure 1. A stainless steel column (L = 23 cm and d_c = 1.1 cm) is filled with a known amount of activated adsorbent particles and placed into the chromatograph oven. Column temperature is thus regulated by the chromatograph regulation system. An inert gas (nitrogen) flows continuously through the column, so as to avoid adsorbent pollution by air. The nitrogen flowrate is controlled by a mass flowmeter, capable of delivering 0−120 cm^3/min of gas.

After passing the flowmeter, the gas stream can either go directly to the chromatograph or pass through the saturator, where it is saturated with the selected hydrocarbon. The hydrocarbon concentration at the saturator is controlled by the saturator temperature, regulated by a cryostat. With this system, it is possible to feed the column with a flow that has a constant and controlled concentration of hydrocarbon, the lowest concentration being limited by the minimum temperature of the cryostat. The efficiency of the saturator was verified: the measured concentration at the outlet of the saturator was in accordance with the theoretical value, calculated using the liquid−vapor equilibrium.

The pulse is produced by injecting a known volume of liquid hydrocarbon with a syringe through the chromatograph injector (septum). The injector is heated at 200 °C so that the evaporation of liquid is instantaneous. To verify system linearity, the injected volume was lowered until no variation of the normalized responses could be seen. This was done for every experiment.

The signal at the output is measured with a thermal conductivity detector (TCD) that was previously calibrated. The TCD was preferred to a flame ionization detector (FID), which is usually used for hydrocarbon compounds, because of the important flows of hydro-

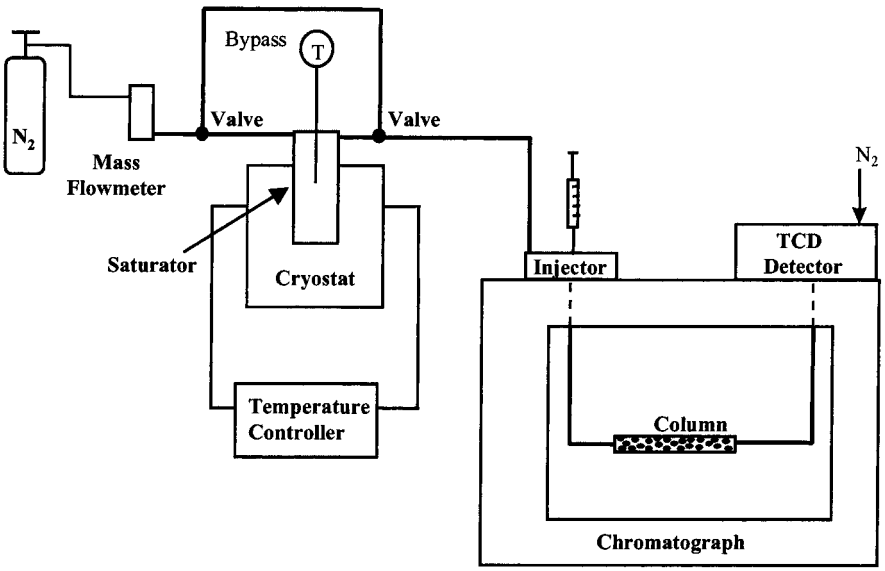

Figure 1. L.A.G.E.P. gas chromatography apparatus.

Table 2. Column and Adsorbent Properties

property	symbol	units	value
bed length	L	m	0.23
bed diameter	d	m	1.1×10^{-2}
bed voidage	ϵ_i	−	0.38
porosity of particles	ϵ_p	−	0.35
% of binder in particles	t	−	0.44
particle radius	R_p	m	1×10^{-3}
crystal radius	R_c	m	2×10^{-6}

carbons to be detected: the FID detector's saturation level is too low. The pressure in the column is always atmospheric pressure. There is no pressure regulation, and the pressure drop through the column is negligible.

Dead volumes of the experimental setup (defined here as the volumes between the injector and the column and between the detector and the column) were determined by measuring the variation of retention time with flow rate in the empty column, and the corresponding dead time was systematically subtracted from the experimental retention time.

Isopentane and 3-methylpentane were purchased from Aldrich and 2,2-dimethylbutane from Fluka. The specified purities are over 99%, and the adsorbates were therefore used without further specification.

The main column and adsorbent properties are listed in Table 2.

Results and Discussion

Adsorption Equilibria. *Adsorption Isotherms.* The adsorption equilibria were determined by the method of moments. From the experimental first moment (or mean retention time), by using eqs 9 and 11, one can evaluate the adsorption's constant K_a, which physically represents the adsorption isotherm's slope at the initial equilibrium or background concentration.

$$K_a(\bar{C},T) = \left.\frac{\partial q^*}{\partial C}\right|_{\bar{C},T} \tag{20}$$

K_a was determined over a wide range of concentration and temperature. Experimental error was evaluated by comparing the values of K_a at different flowrates: the variation was no larger than 1%. The adsorption isotherm was then calculated with the following relation, derived from eq 20:

$$q^*(C,T) = \int_0^C K_a(\bar{C},T)\, d\bar{C} \tag{21}$$

This procedure is summarized in Figure 2, inspired by the paper of Tondeur and al.[3]

Because the variation of K_a with C was known to be nonlinear, particularly at low temperatures and concentrations, the use of classical integration schemes, such as the trapezoidal rule, was not adapted. An interpolation was therefore performed, by assuming that

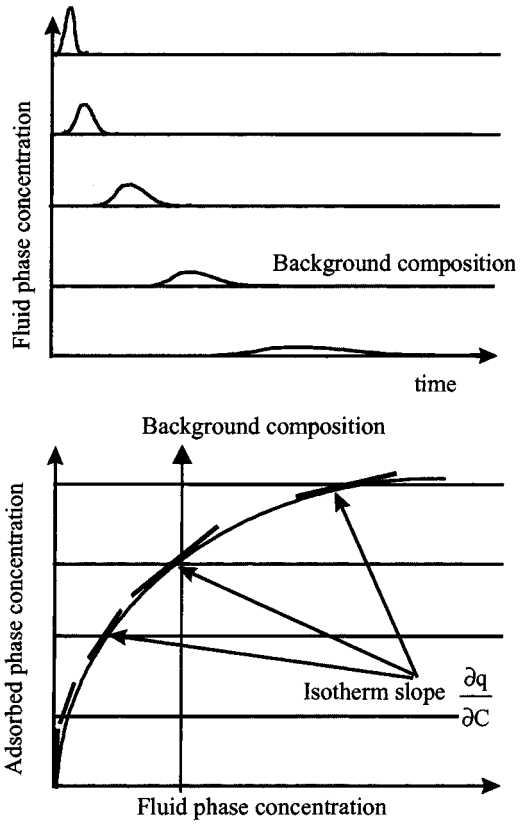

Figure 2. Adsorption isotherm determination from chromatographic response curves.

the evolution of K_a with concentration agrees with Langmuir's model.

$$q^* = q_s \frac{bC}{1 + bC} \tag{22}$$

Equation 20 yields

$$K_a = \frac{q_s b}{(1 + bC)^2} \tag{23}$$

which can be rewritten to give

$$\frac{1}{\sqrt{K_a}} = \sqrt{\frac{b}{q_s}} C + \frac{1}{\sqrt{q_s b}} \tag{24}$$

It was therefore assumed that, between two experimental points, the inverse function of the square root of K_a is linear with concentration.

The above-mentioned method for isotherm determination has a major drawback: the shape of the isotherm depends strongly on the precision of each of the slope values and particularly on the Henry's constant (slope at zero coverage) precision. Any experimental or calculational error can lead to significant inaccuracy in the final determination of the isotherm.

As a consequence, the validity of the data was verified by two techniques: (1) Chromatographic measurements were made with the same apparatus, by changing the impulse perturbation into a step perturbation. The bed, initially empty, was submitted to a concentration step of known composition at its inlet. The output signal was measured and normalized. The quantity adsorbed at the end of the experiment, at equilibrium with the inlet fluid concentration, could be directly calculated as follows:

$$n = \frac{P}{RT} Q_{N_2} \frac{x}{1 - x} \int_0^\infty [1 - F(t)]\, dt \text{ with } F = \frac{C(t)|_{z=L}}{C(t)|_{z=0-}} \tag{25}$$

Equation 25 is derived from a simple mass balance for the whole column. This technique was used only with 3-methylpentane.

(2) Gravimetric uptake measurement were performed with a Setaram TAG 12 thermobalance at the Institut Français du Pétrole.

The resulting isotherms for isopentane, 3-methylpentane, and 2,2-dimethylpentane are shown in Figures 3−5. The isotherms are of "type I" form in Brunauer's classification and were modeled by the Langmuir model.

The data obtained with the three methods (pulse chromatography, step chromatography, and uptake measurements) are in reasonably good agreement (see Figures 3 and 4), except for the isotherm of 2,2-dimethylbutane at 200 °C (see Figure 5) for which adsorbed quantities measured from pulse chromatography experiments are about 50% lower than the quantities measured by the gravimetric technique. The reason for this difference is probably the very slow kinetics of adsorption of 2,2-dimethylbutane in silicalite at this temperature. It is possible that, under these conditions, the local-equilibrium assumption might never be attained. The chromatographic response for 2,2-dimethylbutane at 200 °C and with no background concentration ($\bar{C} = 0$), shown in Figure 6, exemplifies this difficulty: the breakthrough time is nearly 0, and the tailing is so important that the signal is still not stabilized after 1 h. Under these conditions, the isotherm initial slope cannot be precisely determined, so the isotherm of 2,2-dimethylbutane determined by the chromatographic technique is most probably inaccurate.

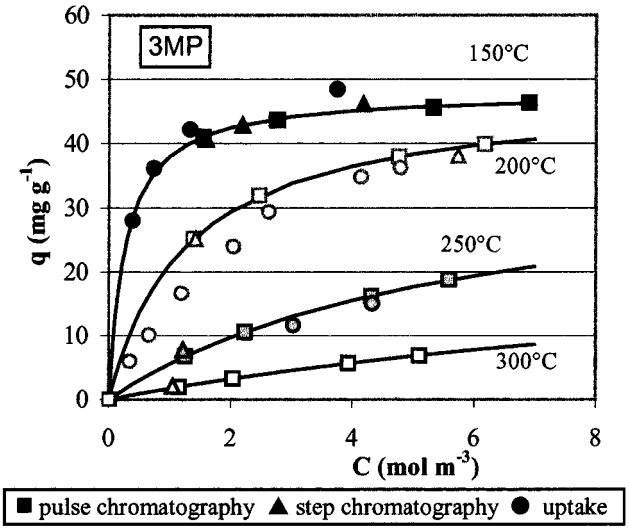

Figure 3. Equilibrium isotherms for 3-methylpentane in silicalite. The points are experimental results, and the lines are calculated from the Langmuir expression (eq 22) with the values of b and q_s listed in Table 3.

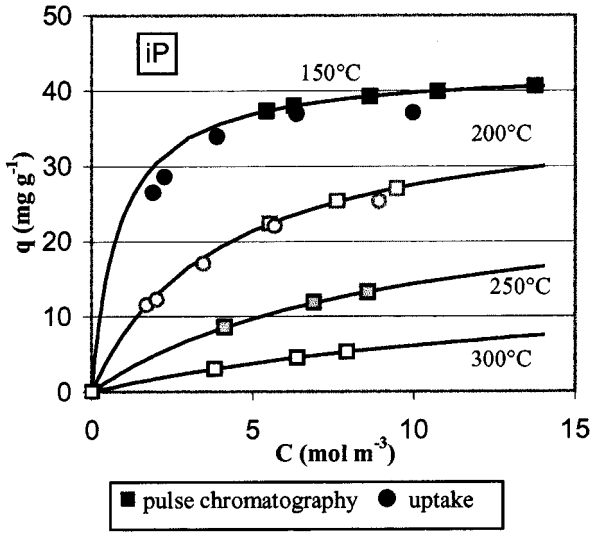

Figure 4. Equilibrium isotherms for isopentane in silicalite. The points are experimental results, and the lines are calculated from the Langmuir expression (eq 22) with the values of b and q_s listed in Table 4.

Once the experimental equilibria were known, the Langmuir parameters were evaluated from a plot of $1/q^*$ vs $1/C$ according to the equation

$$\frac{1}{q^*} = \frac{1}{q_s} + \left(\frac{1}{bq_s}\right)\frac{1}{C} \tag{26}$$

by measuring the slopes and intercepts. The corresponding plot for 3-methylpentane is shown in Figure 7, and the Langmuir parameters values for the three products are given in Tables 3−5.

It is clear from Figure 7 that the Langmuir plots are linear, which means that the experimental points can be correctly represented by the Langmuir model. This

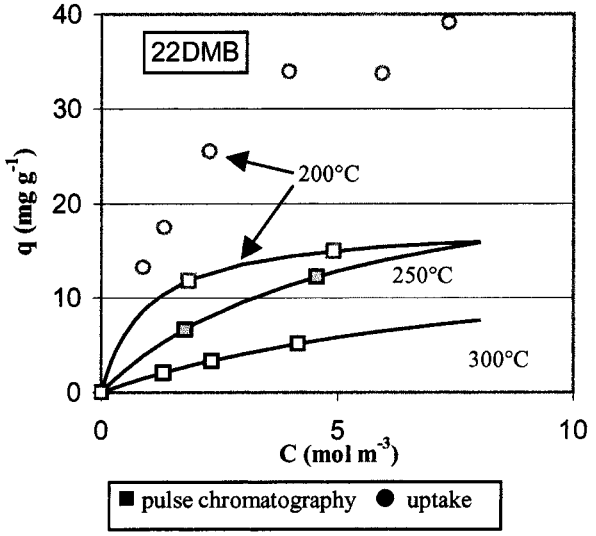

Figure 5. Equilibrium isotherms for 2,2-dimethylbutane in silicalite. The points are experimental results, and the lines are calculated from the Langmuir expression (eq 22) with the values of b and q_s listed in Table 5.

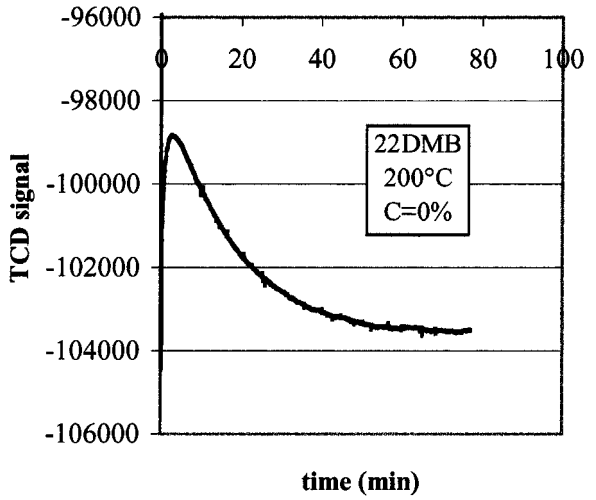

Figure 6. Column response for 2,2-dimethylbutane at 200 °C with no background concentration.

does not imply that the assumptions of the Langmuir model are verified: parameters derived from the Langmuir model often lack physical significance.[12] The decrease of the saturation limit q_s with temperature for 3-methylpentane and isopentane (see Tables 3 and 4) is, for example, not easy to explain, although this phenomenon has frequently been observed.[15,16]

In Tables 3−5, Langmuir parameters obtained in this study are compared with literature results. Our data are in good agreement with the results of Millot et al.[17] However, they differ considerably from the data of Cavalcante and Ruthven.[15] The Langmuir parameters, b, found in this reference are twice as large as our values: under comparable conditions and for the three products, the loading measured by Calvalcante and Ruthven[15] is always substantially larger. Because our results were confirmed by different experimental techniques, it is very improbable that this discrepancy comes from experimental errors. A difference in the nature of the adsorbent studied (Si/Al ratio, defaults of structure) might then be the explanation. It is interesting to note that the tendencies are the same, even if the values are not of the same order of magnitude.

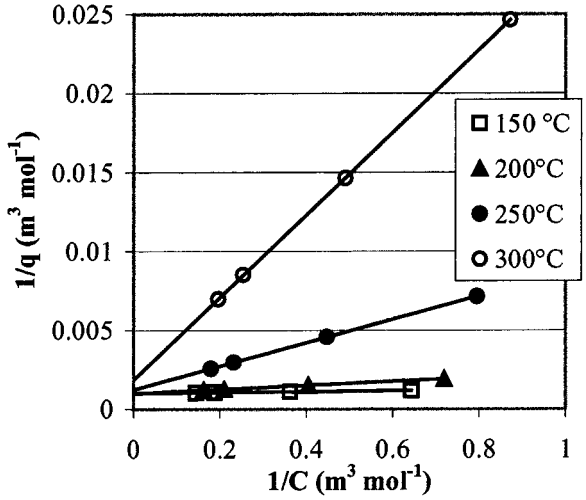

Figure 7. Langmuir plot of equilibrium isotherms for 3-methylpentane in silicalite.

Table 3. Comparison of Langmuir Parameters for 3-Methylpentane

	this study			
	chromatography	uptake	Millot[17 a]	Cavalcante et al.[15]
temp (°C)	q_s (mg/g)	q_s (mg/g)	q_s (mg/g)	q_s (mg/g)
100		53.8	54.1	67.5
150	48.1	53	48.5	60.6
200	48.1	62.4	46.7	54
250	38.2	47.7	34.6	–
300	25.9	–	–	–
temp (°C)	b (m^3/mol)	b (m^3/mol)	b (m^3/mol)	b (m^3/mol)
100	–	28.72	28.28	71.89
150	3.76	2.90	4.39	8.80
200	0.79	0.30	0.80	1.37
250	0.17	0.11	0.19	–
300	0.07	–	–	–

[a] Calculated from experimental data.

Table 4. Comparison of Langmuir Parameters for Isopentane

	this study	
	chromatography	uptake
temp (°C)	q_s (mg/g)	q_s (mg/g)
100	–	47.1
150	43	42.7
200	38.4	35.3
250	27.4	–
300	16.8	–
temp (°C)	b (m^3/mol)	b (m^3/mol)
100	–	2.80
150	1.2	0.88
200	0.25	0.28
250	0.11	–
300	0.06	–

Heats of Adsorption. The adsorption enthalpy of each paraffin in silicalite was calculated from the temperature dependence of the Henry's constants (the isothermal slope at zero coverage) using the van't Hoff equation

$$K'_a(C=0,T) = K'_{a0}(C=0)\exp\left(-\frac{\Delta H}{RT}\right) \qquad (27)$$

where K'_a is the Henry's constant with respect to the fluid-phase partial pressure of hydrocarbon, expressed

Table 5. Comparison of Langmuir Parameters for 2,2-Dimethylbutane

	this study			
	chromatography	uptake	Millot[17] [a]	Cavalcante et al.[15]
temp (°C)	q_s (mg/g)	q_s (mg/g)	q_s (mg/g)	q_s (mg/g)
100	–	44.6	–	–
150	–	–	–	56.1
200	17.8	53.3	59.9	36.1
250	26.0	–	58.4	–
300	16.4	–	–	–
temp (°C)	b (m^3/mol)	b (m^3/mol)	b (m^3/mol)	b (m^3/mol)
100	–	1.26	–	–
150	–	–	–	2.36
200	1.06	0.37	0.7	0.77
250	0.20	–	0.16	–
300	0.11	–	–	–

[a] Calculated from experimental data.

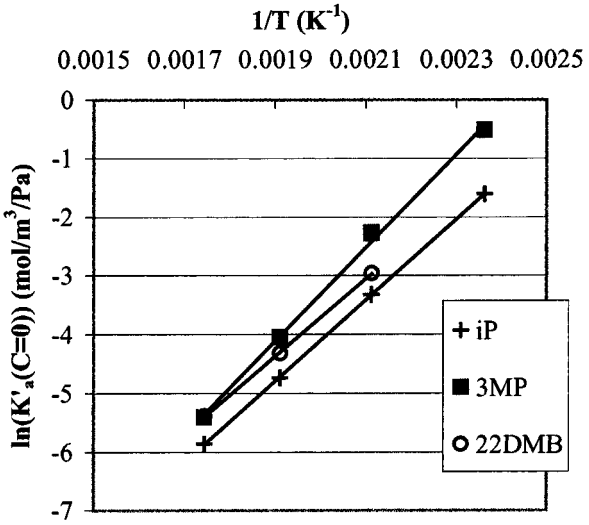

Figure 8. Temperature dependence of Henry's constant for 3-methylpentane, isopentane, and 2,2-dimethylbutane in silicalite.

in mol m^{-3} Pa^{-1}. If the gas phase is ideal, which was assumed in this study, the relationship between K_a and K'_a is

$$K'_a = \frac{K_a}{RT} \tag{28}$$

The plots showing the temperature dependency of K'_a can be seen in Figure 8, which shows that the variation of K'_a with temperature complies with theory (eq 27). The values of ΔH for the three compounds were calculated from the slopes of the straight lines, the van't Hoff plots all having correlation factors R^2 larger than 0.998. A comparison with the results of other studies can be seen in Table 6. Our results are quite consistent with the literature data, but an important dispersion of the experimental values is observed. A very small variation in the slope can lead to a significant error in the adsorption enthalpy value, and it would thus be necessary to have more experimental values of K'_a to determine the enthalpies with a good precision. A general tendency can still be seen: the adsorption enthalpy of 3-methylpentane is greater than those of isopentane and 2,2-dimethylbutane. It is, however, not possible to reach a conclusion about the adsorption enthalpies of these last two products, because results differ greatly depending on the authors.

Table 6. Heats of Adsorption at Zero Coverage, Comparison with Other Studies[a]

product	technique[a]	ref	ΔH (kJ/mol)
3MP	1	this study	−66.4
	1	Denayer et al.[30]	−66.0
	2	Millot[17]	−66.8
	3	Millot[31]	−68.4
	2	Cavalcante and Ruthven[15]	−62.7
	1	Jama et al.[32]	−60
iP	1	this study	−57.4
	1	Denayer et al.[30]	−56.1
	3	Millot[31]	−58.4
22DMB	1	this study	−55.0
	1	Denayer et al.[30]	−63.9
	2	Millot[17]	−58.4
	2	Cavalcante and Ruthven[15]	−54.4

[a] Experimental techniques: 1, chromatographic; 2, gravimetric; 3, temperature-programmed desorption.

Mass Transfer Study. As stated before, the main difficulty for chromatographic pulse analysis, particularly if the moment method is used, is the separation of the effects of the different phenomena on the response dispersion: axial dispersion, film resistance, micropore diffusion, and macropore diffusion. Different methods have been proposed to overcome this problem[12] (use of crystals of different sizes, correlations for estimating mass transfer coefficients, etc.).

In this study, a combination of different techniques is used.

Film Resistance. The importance of film resistance was evaluated using the correlation of Wakao and Kunazkri[18]

$$\mathrm{Sh} = 2 + 1.1\mathrm{Sc}^{1/3}\mathrm{Re}^{0.6} \tag{29}$$

where Sh is the Sherwood number, $\mathrm{Sh} = (2k_pR_p)/D_m$; Sc is the Schmidt number, $\mathrm{Sc} = \mu_f/(\rho_f D_m)$; and Re is the Reynolds number, $\mathrm{Re} = [\rho_f v \epsilon_i (2R_p)]/\mu_f$.

One can see from eq 29 that the minimum value of Sh is 2. As a consequence, the minimum value of k_p calculated from eq 29 is

$$k_{p,\min} = \frac{D_m}{R_p} \tag{30}$$

The molecular diffusivity can be estimated with the Chapman−Enskog equation.[19]

For the lowest temperature studied (T=150 °C), the value of k_p is

$$k_{p,\min} = 1.5 \times 10^{-2}\ \mathrm{m\ s^{-1}}$$

Even with this lowest possible value, the contribution of the film resistance in the expression of the second moment was always found to be less than 1% of the total. Hence, diffusion in the film is assumed to always be negligible for all our experiments.

Axial Dispersion. Axial dispersion can be estimated by measuring the influence of flow velocity on the second moment.[12] Indeed, in the low Reynolds number regime,

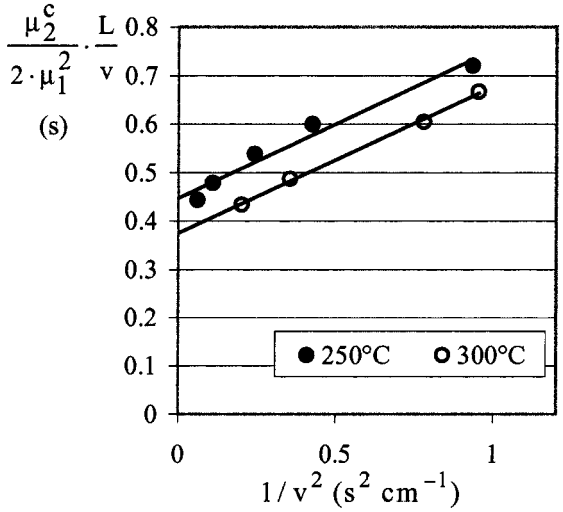

Figure 9. $\mu_2^c/2\mu_1^2(L/v)$ plotted against $1/v^2$ for isopentane at 250 and 300 °C and $\bar{C} = 0\%$.

D_L is essentially independent of velocity, and eq 10 gives

$$\frac{\mu_2^c L}{2\mu_1^2 v} = \frac{D_L}{v^2} + \left(\frac{\epsilon_i}{1-\epsilon_i}\right)\left(\frac{R_p}{3k_p} + \frac{R_c}{3k_t} + \frac{R_c^2}{15KD_c}\right) \times \left[1 + \frac{\epsilon_i}{(1-\epsilon_i)K}\right]^{-2} \quad (31)$$

Therefore a plot of $[(\mu_2^c/2\mu_1^2)(L/v)]$ versus $1/v^2$ should be linear with slope D_L.

The influence of velocity variations on the first and second moments was estimated for isopentane at 250 and 300 °C with no background concentration ($\bar{C} = 0$). The results are plotted in Figure 9. As predicted by eq 31, the plots are basically linear, and in the same velocity range, the slopes are nearly the same for the two temperatures, which means that there is no significant variation of axial dispersion with temperature. The value of the axial dispersion coefficient determined from the slopes is $D_L \approx 3 \times 10^{-5}$ m^2/s.

Those experimental results were compared with correlations. Axial dispersion has been widely studied in the literature, and it has be shown[12] that the effects of molecular diffusion and flow turbulence are approximately additive

$$D_L = \gamma_1 D_m + \gamma_2 2R_p v \quad (32)$$

with

$$\gamma_1 = 0.45 + 0.55\epsilon_i \quad (33)$$

$$\gamma_2 \approx 0.5$$

In the low Reynolds number regime, eq 32 reduces to

$$D_L = \gamma_1 D_m \quad (34)$$

Under our conditions, eq 34 gives $D_L \approx 2 \times 10^{-5}$ m^2/s. Therefore, the axial dispersion coefficient predicted by eq 34 is very close to the experimental value and was therefore used to calculate the value of axial dispersion coefficient for all of the experiments.

Apart from axial dispersion, Figure 9 also provides information on the mass transfer resistance inside the particles and the crystals. The intercept of the line corresponds to the total mass transfer, as can see from eq 31. Assuming that resistance at the particle's surface is negligible, the intercept is

$$\left(\frac{\epsilon_i}{1-\epsilon_i}\right)\left(\frac{R_c}{3k_t} + \frac{R_c^2}{15KD_c}\right)\left(1 + \frac{\epsilon_i}{(1-\epsilon_i)K}\right)^{-2} \quad (35)$$

If the intercept of the line is close to 0, then mass transfer resistances are negligible. In our case, the intercepts are high and temperature-dependent, which suggests that intracrystalline resistance is probably dominant. If micropore diffusion is the limiting step for isopentane at high temperatures, it is very probable that it will also be the case for the other paraffins in the range of temperature studied.

Macropore Diffusion. To separate the effects of macropore and micropore resistances, a parameter estimation study in the time domain was achieved on two experimental curves. The corresponding experimental conditions are detailed in Table 7.

Table 7. Experimental Conditions for the Parameter Estimation Study

experiment no.	1	2
hydrocarbon	22DMB	iP
T (°C)	523	423
C (mol/m^3)	0	0
N_2 flowrate (m^3/s)	3.77×10^{-7}	2.94×10^{-6}

Before the estimation procedure was initiated, a study of the sensitivity of the parameters was performed. A parameter is experimentally identifiable if (1) its sensitivity is not negligible

$$\frac{\partial M}{\partial P_i} \neq 0 \quad (36)$$

and (2) its sensitivity is not proportional to the sensitivity of any other parameter

$$\frac{\partial M(t)}{\partial P_i} \neq A\frac{\partial M(t)}{\partial P_k} \quad \forall\, k \neq i \quad (37)$$

where A is a constant (independent of time).

The sensitivities to the initial parameters of experiment 1 were calculated, and it was found that the two conditions mentioned above are not applicable for all parameters. k_p is not sensitive. The extra and intraparticular porosities ϵ_i and ϵ_p have nearly proportional sensitivities, so that it is not possible to separate their effects: lowering the value of ϵ_i can be compensated by choosing a higher value for ϵ_p. Concerning the parameters k_t and D_c, however, conditions 36 and 37 are fulfilled. They are sensitive, and they do not have the same effects on the curve: k_t is more influent in the short time region (t < 10 min). It was also found that axial dispersion is estimable and that its sensitivity is much more symmetrical than that of the other mass transfer coefficients. A well-known characteristic of the axial dispersion effect is confirmed here.

In Tables 8 and 9 are listed the initial and estimated parameters for both experiments, along with the corresponding first and second moments. The final least-squares criteria, defined by eq 38, where E and M are

Table 8. Initial and Optimized Parameter Values for Experiment 1

parameter	unit	initial value	optimized value
D_L	m^2/s	3×10^{-5}	3.4×10^{-5}
ϵ_i	−	0.37	0.37
ϵ_p	−	0.35	0.35
k_p	m/s	3×10^{-2}	3.2×10^{-2}
K_a	−	57.7	54.9
k_t	m/s	3.64×10^{-7}	1.8×10^{-5}
D_c	m^2/s	2.56×10^{-15}	1.4×10^{-15}
μ_1	s	1380	1380
μ_2	s^2	2.51×10^{6}	2.47×10^{6}
least-squares criteria J	−	3×10^{-6}	2.4×10^{-7}

Table 9. Initial and Optimized Parameter Values for Experiment 2

parameter	unit	initial value	optimized value
D_L	m^2/s	9.22×10^{-5}	9.76×10^{-5}
ϵ_i	−	0.37	0.37
ϵ_p	−	0.35	0.34
k_p	m/s	2×10^{-2}	2×10^{-2}
K_a	−	695.2	677.9
k_t	m/s	1.82×10^{-6}	4.49×10^{-6}
D_c	m^2/s	9.74×10^{-16}	1.46×10^{-15}
μ_1	s	2124	2088
μ_2	s^2	5.81×10^{6}	5.48×10^{6}
least-squares criteria J	−	4.16×10^{-6}	1.35×10^{-7}

respectively the experimental and model output, are also recorded in those tables.

$$J = \frac{\int_0^\infty [E(t) - M(t,C)]^2 \, dt}{n_p} \tag{38}$$

The least-squares criteria is divided by 10 between the initial and the estimated value by optimization. As can be seen in Tables 8 and 9, the optimized curves have lower micropore diffusion coefficients and higher macropore diffusion coefficients, whereas their first and second moments are almost constant. This result shows once again that the influence of the different kinetic parameters on the shape of the curve is different and that the moment analysis, if restricted to the first two moments, is not sufficient. The correct way to use the moment analysis is to previously determine the relative importance of the different mass transfer parameters with a time domain analysis. In our case, time domain fitting allowed us to conclude that the experimental curves cannot be represented by the model if macropore resistance is too important. The final value of k_t for experiment 1 is so large that its contribution to the second moment is under 2%. For this experiment, macropore resistance is negligible compared to micropore resistance. For experiment 2 however, the final contribution of the optimized parameter k_t to the second moment is 25%, which is not negligible anymore.

Particle Tortuosity Evaluation. If the value of the macropore resistance is known, then it is theoretically possible to calculate the tortuosity factor τ by matching the experimental value of the macropore diffusivity with the corresponding correlations. However, k_t is not a diffusivity but a lumped parameter. The "true" diffusion coefficient D_p has to be calculated by assuming that the contribution of both parameters to the second moment are the same[12]

$$\frac{R_c}{3k_t} = \frac{R_p^2}{15\epsilon_p D_p} \tag{39}$$

where the term on the left-hand side represents the k_t contribution and the term on the right-hand side represents the D_p contribution. Equation 39 gives

$$D_p = \frac{3R_p^2 k_t}{15\epsilon_p R_c} \tag{40}$$

According to eq 40, the experimental value of D_p for experiment 2 is

$$D_p = 1.2 \times 10^{-6} \ m^2/s$$

The theoretical value of D_p is

$$D_p = \frac{1}{\tau} \frac{1}{\frac{1}{D_K} + \frac{1}{D_m}} \tag{41}$$

where D_K is the Knudsen diffusion coefficient and D_m is the molecular diffusion coefficient.

The tortuosity factor is therefore (eqs 40 and 41)

$$\tau = \frac{15\epsilon_p R_c}{3R_p^2 k_t} \frac{1}{\frac{1}{D_K} + \frac{1}{D_m}} \tag{42}$$

where[12]

$$D_K = 9700 r_{pore} \left(\frac{T}{MW}\right)^{1/2} \tag{43}$$

Under the experimental conditions of experiment 2, eq 43 gives $D_K = 6.14 \times 10^{-6}$ m^2/s. Finally, the value of τ can be estimated from eq 42, giving $\tau = 3.5$. This tortuosity factor is quite consistent with the values that can be found in the literature.[20−22] The estimated value of k_t is therefore realistic. The estimated tortuosity factor was used in the rest of this study to estimate the values of k_t for each experiment. It has been shown that the influence of the determination of k_t on the final value of D_c is generally not very large, and an approximation of k_t should therefore be negligible concerning the final precision of D_c.

Micropore Diffusion. The micropore effective diffusivity D_c was estimated using the experimental second moment. The effect of film resistance was neglected, axial dispersion was estimated using eq 34, and the macropore resistance parameter k_t was estimated using eq 41 with $\tau = 3.5$. The variation of D (self-diffusion coefficient) with temperature is plotted in Figure 10 for the three hydrocarbons. As expected, the experimental results follow an Arrhenius law

$$\ln[D_c(\bar{C}=0)] = \ln(D) = \ln(D^*) - \frac{E_a}{RT} \tag{44}$$

with correlation factors R^2 larger than 0.99 for iP and 22DMB and equal to 0.94 for 3MP. The slopes of the lines yield the activation energy E_a, and the intercept the preexponential term. The values of E_a and D^* are listed in Table 10, along with literature results. Activa-

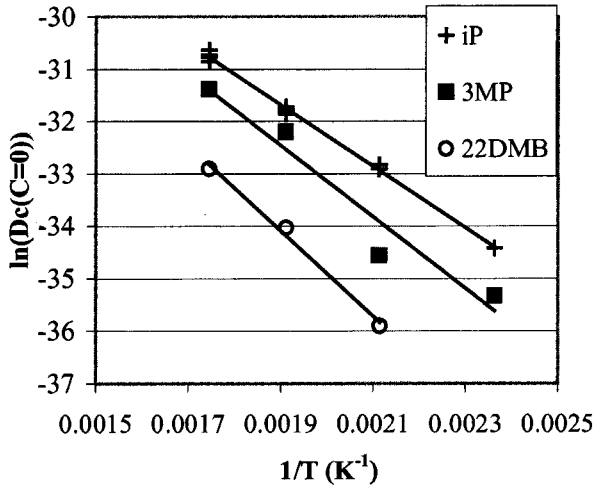

Figure 10. Variation of self-diffusivity with temperature for 3-methylpentane, isopentane, and 2,2-dimethylbutane.

Table 10. Energies of Activation and Preexponential Diffusion Coefficients, Comparison with Other Studies

	ref	technique[a]	E_a (kJ/mol)	D^* (m^2/s)
iP	this study	1	46	5.9×10^{-10}
	Xiao and Wei[29]	2	32	3.8×10^{-8}
3MP	this study	1	56	2.7×10^{-9}
	Cavalcante and Ruthven[1]	2	58	1.9×10^{-5}
	Millot[33]	3	50	4×10^{-7}
	Jama et al.[32]	4	28	8.3×10^{-10}
22DMB	this study	1	68	8.5×10^{-9}
	Xiao and Wei[29]	2	70	1.1×10^{-7}
	Cavalcante and Ruthven[1]	2	77	2.6×10^{-6}
	Post et al.[24]	1	64	7.4×10^{-10}

[a] Experimental techniques: 1, chromatographic; 2, gravimetric; 3, membrane; 4, wall-coated column.

tion energies found in this study are rather consistent with literature data, and the general tendency is E_a(22DMB) > E_a(3MP) > E_a(iP). As was mentioned before with regard to heats of adsorption, the derived value of the activation energy is very sensitive to any uncertainty in the slope of the plot, and a great quantity of precise experimental measurements are therefore necessary to determinate the activation energy with accuracy. The preexponential term shows a great deal of scatter. This is a classical result of literature: the measured diffusivities in zeolites differ greatly depending on the experimental technique and the crystal studied. We will not discuss this point extensively; Karger and Ruthven[23] have thoroughly reviewed the subject. They suggested that the discrepancy between the data is due to the different time scales of the experimental techniques: the time scale of microscopic NMR measurements is on the order of a few milliseconds, whereas a macroscopic measure can last for more than hour. Even though the data contained in Table 10 have all been measured with macroscopic techniques, a difference is still noticeable between the results obtained with the different techniques: chromatography-determined diffusivities are always lower than uptake curve and membrane data.

Another possible explanation is that the chemical composition of the zeolite is not exactly the same for each study, depending on the origins of the adsorbents. It is known, for example, that the Si/Al ratio has an influence on diffusivity.[24] Also, defects in the structure of the zeolites are not well controlled[25] and could have a significant effect on the diffusivities of the slower diffusing species.[26]

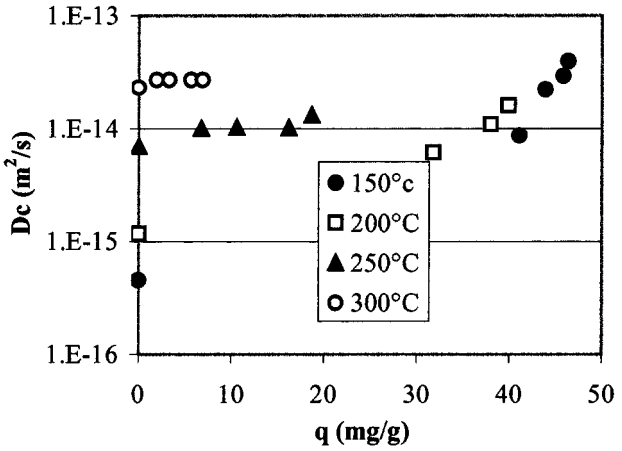

Figure 11. Variation of effective diffusivity with temperature and concentration for 3-methylpentane.

Whatever the reference, the following trend is observed for the diffusivities: isopentane > 3-methylpentane > 2,2-dimethylbutane. As was found for equilibrium data, the tendencies are the same even if the amplitudes are quite different.

The variation of the effective diffusivity D_c with the adsorbed-phase concentration was studied for the three hydrocarbons. As an example, the results for 3-methylpentane are plotted in Figure 11. Effective diffusivities have the expected trends: (1) the higher the temperature, the higher the self-diffusion coefficient, in accordance with eq 44; and (2) for a given temperature, the diffusivity increases with adsorbed-phase concentration.

The tendencies described by points 1 and 2 were observed for the three species. The increase in diffusivity is, of course, more obvious for the lower temperature, for which the adsorbed quantity is greater.

According to Darken's law, if the equilibrium is represented by the Langmuir model and if the self-diffusion coefficient D does not vary with concentration, then

$$\frac{D_c}{D} = \frac{1}{1-\bar{\theta}} = \Gamma \qquad (45)$$

over the whole adsorbed-phase concentration range. Γ is called the thermodynamic correction factor.

To test the validity of eq 45 for our system, D_c/D was plotted as a function of $\bar{\theta}$ on the same graph for the three products and for all temperatures (Figure 12). It is clear from Figure 12 that the three hydrocarbons follow the same trend: the variation in diffusivity with the adsorbed fraction is remarkably similar. This trend follows eq 45 if $\bar{\theta} < 0.7$, but for greater values of $\bar{\theta}$, the measured diffusivities are higher than predicted. The following phenomena might explain this observation: (1) The self-diffusion coefficient D might vary with concentration in the adsorbed phase. Assuming that the observed experimental deviation from Darken's law is solely due to a change in self-diffusivity, the theoretical variation of self-diffusivity with concentration was calculated and plotted in Figure 13. One can see from this figure that self-diffusivity is constant up to $\bar{\theta} = 0.7$ and increases

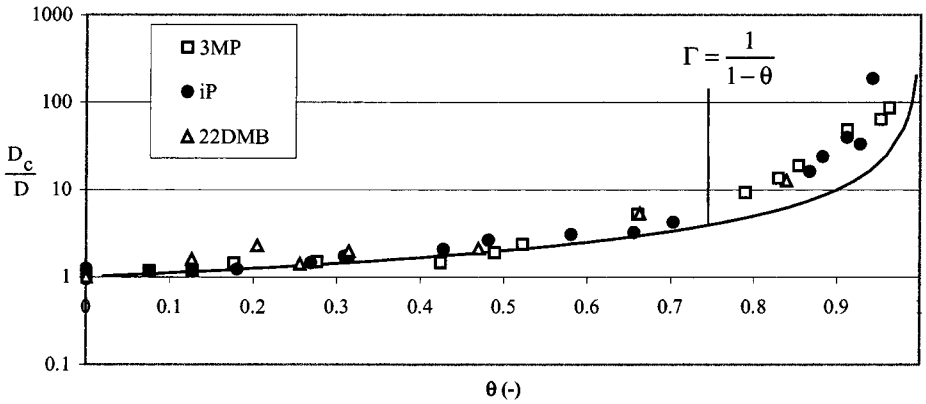

Figure 12. Comparison between the experimental corrected diffusivities and the theoretical correction factor.

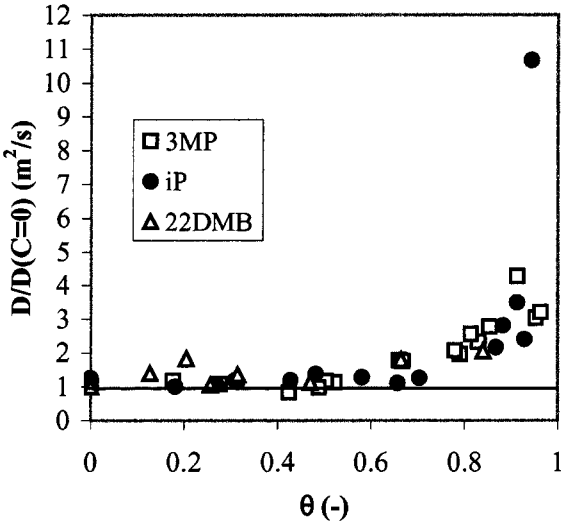

Figure 13. Variation of self-diffusivity with concentration in the adsorbed phase.

afterward. When the number of molecules in the lattice of the zeolite increases, interactions between neighboring molecules could become significant. According to Reed and Ehrlich,[27] a repulsive force can then result in an increase of D with $\bar{\theta}$. Wei[28] suggests that, at high loading, the energy of activation would decrease because of the deformation of the solid structure. This would result in an increase in self-diffusivity when the diameter of the molecules is close to the diameter of the pores and to a decrease in diffusivity in the opposite case.

(2) In the high occupancy region, the diffusional time constant becomes less and less significant. An initially nonlimiting resistance, such as surface diffusion, might then become significant. For higher loadings, the diffusion coefficient value might therefore be a "combination" between micropore and surface diffusion, resulting in an apparent rise of the micropore diffusivity. The increase in self-diffusivity measured for $\bar{\theta} > 0.7$ would, in this case, have no real physical meaning.

Very few data are present in the literature concerning the diffusivity variations of isopentane, 2,2-dimethylbutane, and 3-methylpentane with concentration. Xiao and Wei[29] found that isopentane diffusivity is constant for a loading less than 4 molecules per cell (50 mg/g) and rises significantly above this value. However, the measurements were made at 24 °C, well under the temperatures studied here.

Conclusion

Adsorption isotherms and effective diffusivities were measured for isopentane, 2,2-dimethylbutane, and 3-methylpentane for temperatures between 150 and 300 °C in silicalite using the inverse chromatography technique. Equilibrium results are in good agreement with literature, except for the data of Cavalcante and Ruthven.[15] It is interesting to notice that, with a well-known zeolite such as silicalite, discrepancies in equilibrium data can still exist between different studies. Effective diffusivities were found to increase with adsorbed-phase concentration following Darken's law up to 70% of total loading (4 molecules/cell). Above this value, values predicted with Darken's law are lower than the experimental data. The same trend was observed for all hydrocarbons. The energies of activation obtained from the variation of self-diffusivities with temperature are in good agreement with literature data.

Self-diffusivity values exhibit the following expected tendency: isopentane > 3-methylpentane > 2,2-dimethylbutane. They are generally in poor agreement with literature results. The discrepancy of the diffusivity data obtained with different experimental techniques and/or different adsorbent samples is not surprising and indicates that the data given in this work might not be adapted to experimental systems excessively different from the one used in this study. This illuminates the great quantity of work that still has to be done in the field, particularly in studying the relation between adsorption and diffusion phenomena.

Nomenclature

C_1-C_8 = groups of parameters specified in Table 1
b = "Langmuir" parameter (m^3/mol)
C = fluid-phase concentration (mol/m^3)
$\hat{C}$ = difference between initial thermodynamic equilibrium state and current fluid concentrations, $\hat{C} = C - \bar{C}$ (mol/m^3)
$\bar{C}$ = fluid-phase concentration at the initial thermodynamic equilibrium state (mol/m^3)
C_p = macropore concentration (mol/m^3)
C_p^* = concentration defined by $C_{pj}^* = q_j/K_j$ (mol/m^3)
D = self-diffusion coefficient (m^2/s)
D^* = preexponential factor from eq 44 (m^2/s)
D_c = micropore effective diffusivity (m^2/s)
D_K = Knudsen diffusion coefficient (m^2/s)
D_L = axial dispersion coefficient (m^2/s)
D_m = molecular diffusion coefficient (m^2/s)
D_p = macropore diffusion coefficient (m^2/s)
d_p = particle mean diameter (m)

E = experimental output
E_a = activation energy (J/mol)
F = column step output (−)
ΔH = molar heat of adsorption (J/mol)
J = mean square criteria defined by eq 38 (−)
k_p = mass transfer coefficient around particles (m/s)
k_t = mass transfer coefficient around crystals (m/s)
K = adsorption constant defined by eq 11 (−)
K_a = slope of the adsorption isotherm based on the crystal volume and a function of the fluid-phase concentration, defined by eq 20 (−)
K'_a = slope of the adsorption isotherm based on the crystal volume and a function of the partial pressure in the fluid phase, defined by eq 28 (mol/m^3/Pa)
K'_{a0} = preexponential factor of eq 27 (mol/m^3/Pa)
L = column length (m)
L_p = particle mean length (m)
M = output of a given model
MW = molecular weight (g/mol)
n = number of moles adsorbed (mol)
n_p = number of experimental points (−)
q = adsorbed-phase concentration (mol/m^3 or mg/g)
$\hat{q}$ = difference between initial thermodynamic equilibrium state and current adsorbed-phase concentrations, $\hat{q} = q - \bar{q}$ (mol/m^3 or mg/g)
$\bar{q}$ = adsorbed-phase concentration at the initial thermodynamic equilibrium state (mol/m^3 or mg/g)
q^* = adsorbed-phase concentration in equilibrium with macropore (mol/m^3 or mg/g)
q_s = adsorbed-phase concentration at saturation (mol/m^3 or mg/g)
P = column pressure (Pa)
P, P' = given parameter vectors
Q = volumetric flow rate (m^3/s)
R = ideal gas constant (J mol^{-1} K^{-1})
R_c = crystal mean radius (m)
R_p = particle mean radius (m)
r_p = radial particle coordinate (m)
r_c = radial crystal coordinate (m)
r_{pore} = mean macropore radius (m)
T = temperature (K)
t = mass ratio of binder in particle (−)
t' = additional retention time due to dead volumes (s)
u = superficial velocity (m/s)
v = interstitial velocity (m/s)
x = fluid-phase molar fraction of adsorbate (−)
z = axial column coordinate (m)

Subscripts

0 = at $z = 0$
p = concerning particles
c = concerning crystals
min = minimum value

Greek Letters

ϵ_{12} = Lennard-Jones energy (J)
ϵ_i = interstitial porosity (−)
ϵ_p = macroporosity (−)
μ_f = fluid-phase viscosity (Pa s)
μ_1 = mean retention time or first moment (s)
μ_2 = second moment (s^2)
μ_2^c = standard deviation $\mu_2^c = \mu_2 - \mu_1^2$ (s^2)
ρ = dimensionless space variable defined by $\rho = r_c/R_c$ (−)
ρ_f = fluid-phase density (kg m^{-3})
θ = adsorbed-phase fractional saturation $\theta = q/q_s$ (−)
τ = tortuosity factor (−)
σ = characteristic length (Lennard-Jones) (Å)
Ω^* = diffusion collision integral (−)
γ_1 and γ_2 = coefficients defined by eq 33 (−)
ζ = dimensionless space variable defined by $\zeta = z/L$ (−)
Γ = thermodynamical correction factor defined by eq 45 (−)

Literature Cited

(1) Cavalcante, C. L., Jr.; Ruthven, D. M. Adsorption of branched and cyclic paraffins in silicalite. 2. Kinetics. *Ind. Eng. Chem. Res.* **1995**, *34* (1), 185−191.

(2) Volles, W. K. Adsorption and Isomerization of Normal and Monomethyl Paraffins. U.S. Patent 5,055,634, 1991.

(3) Tondeur, D.; Kabir, H.; Luo, L. A.; Granger, J. Multicomponent adsorption equilibria from impulse response chromatography. *Chem. Eng. Sci.* **1996**, *51* (15), 3781−3799.

(4) Hyun, S. H.; Danner, R. P. Determination of gas adsorption equilibria by the concentration pulse technique. *AIChE J. Symp. Ser.* **1982**, *78*, 19−28.

(5) Hufton, J. R.; Danner, R. P. Chromatographic study of alkanes in silicalite: equilibrium properties. *AIChE J.* **1993**, *39* (6), 954−961.

(6) Hufton, J. R.; Danner, R. P. Chromatographic Study of Alkanes in Silicalite: Transport Properties. *AIChE J.* **1993**, *39* (6), 962−974.

(7) Wakao, N.; Kaguei, S.; Smith, J. M. Adsorption chromatography measurements. parameter determination. *Ind. Eng. Chem. Fundam.* **1980**, *19*, 363−367.

(8) Boniface, H. A.; Ruthven, D. M. The use of higher moments to extract transport data from chromatographic adsorption experiments. *Chem. Eng. Sci.* **1985**, *40* (8), 1401−1409.

(9) Shah, D. B.; Oey, N. K. Application of method of moments to highly skewed responses. *Zeolites* **1988,** *8*, 404−408.

(10) Tayakout-Fayolle, M.; Jolimaître, E.; Jallut C. Consequence of structural identifiability properties on state-model formulation for linear inverse chromatography. *Chem. Eng. Sci.* **2000**, *55* (15), 2945−2956.

(11) Fahim, M. A.; Wakao, N. Parameter estimation from tracer response measurements. *Chem. Eng. Sci.* **1982**, *25*, 1−8.

(12) Ruthven, D. M. *Principle of Adsorption and Adsorption Processes*; John Wiley & Sons: New York, 1984.

(13) Walter, E.; Pronzato, L. Qualitative and quantitative experiment design for phenomenological models—A survey. *Automatica* **1990**, *26* (2), 195−213.

(14) Jolimaitre, E. *Etude et modélisation de l'adsorption et du transfert de matière dans les zéolithes de structure MFI*. Ph.D. Thesis: University of Lyon I, Lyon, France, 1999.

(15) Cavalcante, C. L., Jr.; Ruthven, D. M. Adsorption of branched and cyclic paraffins in silicalite. 1. Equilibrium. *Ind. Eng. Chem. Res.* **1995**, *34* (1), 177−184.

(16) Ruthven, D. M.; Kaul, B. K. Adsorption of aromatic hydrocarbons in NaX zeolite. 1. Equilibrium. *Ind. Eng. Chem. Res.* **1993**, *32*, 2047−2052.

(17) Millot, B.; Méthivier, A.; Jobic, H. Modelling of adsorption equilibria of C_4 to C_7 alkanes in MFI type zeolites. *Proc. 6th Int. Conf. Fundam. Adsorpt.* **1998**, 273−278.

(18) Wakao, N.; Funazkri, T. Effect of fluid dispersion coefficients on particle-to-fluid mass transfer coefficients in packed beds. Correlation of Sherwood numbers. *Chem. Eng. Sci.* **1978**, *33*, 1375−1384.

(19) Reid, R. C.; Prausnitz, J. M.; Poling, B. E. *The properties of gases and liquids*, 4th ed.; McGraw-Hill: New York, 1987.

(20) Garcia-Ochoa, F.; Santos, A. Effective diffusivity under inert and reaction conditions. *Chem. Eng. Sci.* **1994**, *49* (18), 3091−3102.

(21) Hashimoto, K.; Smith, J. M. Macropore diffusion in molecular sieve pellets by chromatography. *Ind. Eng. Chem. Fundam.* **1973**, *12* (3), 353−359.

(22) Wang, C. T.; Smith, J. M. Tortuosity factors for diffusion in catalyst pellets. *AIChE J.* **1983**, *29* (1), 132−136.

(23) Kärger, J.; Ruthven, D. M. On the comparison between macroscopic and nmr measurements of intracrystalline diffusion in zeolites. *Zeolites* **1989**, *9*, 267−281.

(24) Post, M. F. M.; Van Amstel, J.; Kouwenhoven, H. W. Diffusion and catalytic reaction of 2−2,dimethyl butane in ZSM-5 zeolite. *Proc. 6th Int. Zeolite Conf.* **1984**, 517.

(25) Chezeau, J. M.; Delmotte, L.; Guth, J. L.; Gabelica, Z. Influence of synthesis conditions and postsynthesis treatments on the nature and quantity of structural defects in highly siliceous MFI zeolites: a high-resolution solid-state ^{29}Si NMR study. *Zeolites* **1991**, *11*, 598−606.

(26) Hufton, J. R.; Ruthven, D. M.; Danner, R. P. Adsorption and diffusion of hydrocarbons in silicalite at very low concentration: Effect of defect sites. *Microporous Mater.* **1995**, *5*, 39−52.

(27) Reed, D. A.; Ehrlich, G. Surface diffusion, atomic jump and thermodynamics. *Surf. Sci.* **1981**, *102*, 588−609.

(28) Wei, J. *Materials Res. Soc. Symp. Proc.* **1988**, *111*, 413.

(29) Xiao, J.; Wei, J. Diffusion mechanisms of hydrocarbons in zeolites. II. Analysis of experimental observations. *Chem. Eng. Sci.* **1992**, *47* (5), 1143−1159.

(30) Denayer, J. F.; Souverijns, W.; Jacobs, P. A.; Martens, J. A.; Baron, G. V. High-temperature low-pressure adsorption of branched C_5−C_8 alkanes on Zeolite Beta, ZSM-5, ZSM-22, Zeolite Y, and Mordenite. *J. Phys. Chem. B* **1998**, *102*, 4588−4597.

(31) Millot, B.; Méthivier, A.; Jobic, H.; Clemençon, I.; Rebours B. Adsorption of branched alkanes in silicalite. 1: A temperature-programmed-equilibration study. *Langmuir* **1999**, *15* (7), 2534−2539.

(32) Jama, M. A.; Delmas, M. P. F.; Ruthven, D. M. Diffusion of linear and branched C_6 hydrocarbons in silicalite studied by the wall-coated capillary chromatographic method. *Zeolites* **1997**, *18*, 200−204.

(33) Millot, B. *Etude du transport d'hydrocarbures saturés dans des membranes zéolithiques de structure MFI.* Ph.D. Thesis: University of Lyon I, Lyon, France, 1998.

Received for review May 11, 2000
Revised manuscript received October 17, 2000
Accepted October 23, 2000

IE0004693